THE JOURNAL OF BIOLOGICAL CHEMISTRY VOL. 282, NO. 49, pp. 36057–36067, December 7, 2007

Conformational Variability of the Glycine Receptor M2 Domain in Response to Activation by Different Agonists*

Received for publication, August 6, 2007, and in revised form, September 20, 2007 Published, JBC Papers in Press, October 2, 2007, DOI 10.1074/jbc.M706468200

Stephan A. Pless[‡1], **Mohammed I. Dibas**[§2], **Henry A. Lester**[§], **and Joseph W. Lynch**[‡3]

From the [‡]*School of Biomedical Sciences, University of Queensland, Brisbane, Queensland 4072, Australia and the* [§]*Division of Biology, California Institute of Technology, Pasadena, California 91125*

Models describing the structural changes mediating Cys loop receptor activation generally give little attention to the possibility that different agonists may promote activation via distinct M2 pore-lining domain structural rearrangements. We investigated this question by comparing the effects of different ligands on the conformation of the external portion of the homomeric α1 glycine receptor M2 domain. Conformational flexibility was assessed by tethering a rhodamine fluorophore to cysteines introduced at the 19′ or 22′ positions and monitoring fluorescence and current changes during channel activation. During glycine activation, fluorescence of the label attached to R19′C increased by ~20%, and the emission peak shifted to lower wavelengths, consistent with a more hydrophobic fluorophore environment. In contrast, ivermectin activated the receptors without producing a fluorescence change. Although taurine and β-alanine were weak partial agonists at the α1R19′C glycine receptor, they induced large fluorescence changes. Propofol, which drastically enhanced these currents, did not induce a glycine-like blue shift in the spectral emission peak. The inhibitors strychnine and picrotoxin elicited fluorescence and current changes as expected for a competitive antagonist and an open channel blocker, respectively. Glycine and taurine (or β-alanine) also produced an increase and a decrease, respectively, in the fluorescence of a label attached to the nearby L22′C residue. Thus, results from two separate labeled residues support the conclusion that the glycine receptor M2 domain responds with distinct conformational changes to activation by different agonists.

Glycine receptor (GlyR)[4] chloride channels mediate inhibitory neurotransmission in the central nervous system (1). They comprise an assembly of five subunits that are each composed of a large N-terminal extracellular ligand-binding domain and four transmembrane α-helices (M1–M4). Cryo-electron microscopy images of the homologous *Torpedo electropax* nicotinic acetylcholine receptor (nAChR) transmembrane region reveals that the pore-lining M2 domains are kinked radially inward to form a central constriction at the membrane midpoint (2). There is currently a great deal of interest in understanding how M2 domains move to open the channel. Although the original model proposed a drastic rotation of M2 domains about their long axes (3), more recent evidence suggests that there is little if any rotation during receptor activation (4–6). The precise nature of the structural change remains a matter for debate.

The central pore kink is likely to introduce a degree of structural discontinuity because the hydrogen bonds responsible for maintaining α-helix rigidity are most likely broken. The kink may therefore act as a swivel enabling the outer half of M2 to move asynchronously with the inner half, where the gate is most likely positioned. Indeed, several lines of evidence suggest gating is mediated by a backbone rearrangement at this midpoint (7–10). In addition, a rate equilibrium free energy state analysis shows that the M2–M3 domain is positioned midway along the agonist-induced "conformational wave" that extends from the ligand binding domain to the gate (11). These considerations imply that the outer part of M2 should be an informative place to investigate the structural basis of receptor activation, as the movements in this region should not reflect either those occurring at the ligand binding site or the activation gate. Thus, in this study we probe conformational changes at the 19′ and 22′ residues, near the external end of M2.

Current models of Cys loop receptor activation consider only structural changes associated with transitions from the resting closed state to the agonist-induced open state (5, 6, 12, 13). Relatively little attention has been given to the possibility that different agonists and pharmacological modulators may promote different structural conformations in the pore region. However, it has been suggested on the basis of substituted cysteine accessibility studies that the pore blocker, picrotoxin, can change the conformation of the outer GlyR pore region suggesting in turn that it may interact allosterically with agonist-induced conformational changes (14). Our aim is to investigate the conformational changes induced by agonists, antagonists, and allosteric modulators by covalently labeling different residues near the extracellular M2 boundary with the sulfhydryl-reactive fluorophores, methanethiosulfonate-rhodamine (MTSR) and tetramethylrhodamine-maleimide (TMRM), and

* This work was supported in part by the National Health and Medical Research Council of Australia and by National Institutes of Health Grant NS-11756. The costs of publication of this article were defrayed in part by the payment of page charges. This article must therefore be hereby marked "*advertisement*" in accordance with 18 U.S.C. Section 1734 solely to indicate this fact.
[1] Supported by an International Postgraduate Research Scholarship from the University of Queensland.
[2] Supported by an National Research Service Award from the National Institutes of Health.
[3] Supported by a National Health and Medical Research Council of Australia Senior Research Fellowship. To whom correspondence should be addressed: School of Biomedical Sciences, University of Queensland, Brisbane, Queensland 4072, Australia. Tel.: 617-3365-3157; Fax: 617-3365-1766; E-mail: j.lynch@uq.edu.au.
[4] The abbreviations used are: GlyR, glycine receptor; MTSR, methanethiosulfonate-rhodamine; M1–M4, transmembrane segments 1–4; nAChR, nicotinic acetylcholine receptor; TMRM, tetramethylrhodamine-maleimide; VCF, voltage-clamp fluorometry; WT, wild type; TRITC, tetramethylrhodamine isothiocyanate.

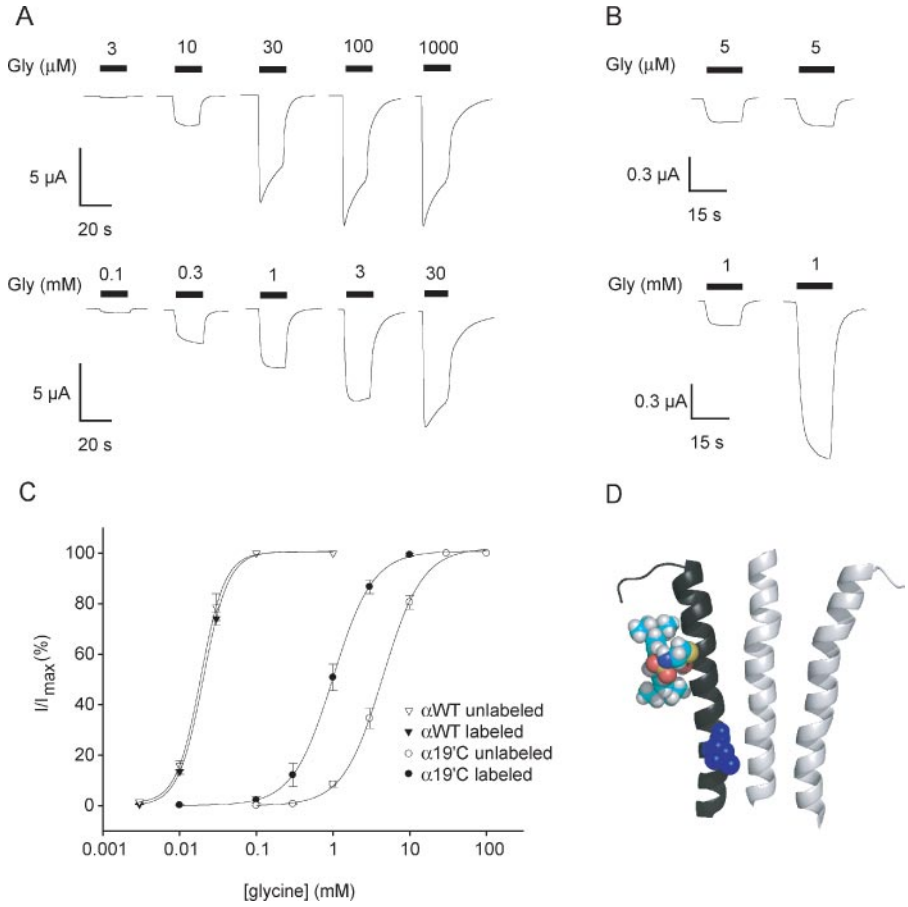

FIGURE 1. **Effects of MTSR labeling on α1WT and α1R19′C GlyRs.** *A,* glycine-evoked currents recorded from oocytes injected with α1WT (*upper panel*) and α1R19′C (*lower panel*) after labeling with MTSR. *B,* glycine-evoked currents recorded from oocytes injected with α1WT (*upper panel*) or α1R19′C (*lower panel*) before (*left panel*) and after (*right panel*) labeling with MTSR. *C,* glycine dose-response relations for α1WT and α1R19′C before and after labeling with MTSR. *Black horizontal bars* indicate duration of glycine application. All concentrations are in mM. *D,* ribbon model of three pore-facing nAChR M2 helices and their M2–M3 linkers in *black* and *gray* (based on Protein Data Bank code 2BG9). A space filling model of the 9′ leucine is shown in *dark blue.* A space filling model of MTSR molecule is tethered to the 19′ position (approximate orientation based on H. A. Lester and M. I. Dibas, manuscript in preparation). Color code is as follows: *white,* hydrogen; *light blue,* carbon; *red,* oxygen; *dark blue,* nitrogen; and *yellow,* sulfur.

simultaneously measuring current changes and fluorescence changes (15, 16). This approach has been employed so far in only a few studies on Cys loop receptors (15, 17, 18). A particular advantage of the GlyR is that it displays little or no desensitization thereby facilitating the quantitation of ligand-induced fluorescence spectral shifts.

EXPERIMENTAL PROCEDURES

Chemicals—Glycine, $CaCl_2$, $MgCl_2$, KCl, NaCl, and glycerol were all purchased from Ajax Finechem (Seven Hills, New South Wales, Australia). HEPES was purchased from Amresco (Solon, OH). Sulforhodamine methanethiosulfonate (MTSR, Toronto Research Chemicals, North York, Ontario, Canada) and tetramethylrhodamine-5-maleimide (TMRM, Invitrogen) were dissolved in dimethyl sulfoxide (Me_2SO) and stored at −20 °C. Picrotoxin (Sigma), ginkgolide C (Tauto Biotech Co., Shanghai, China), and ivermectin (Sigma) were dissolved in Me_2SO and stored at −20 °C. Propofol (2,6-diisopropylphenol) was purchased from Sigma and stored at 4 °C. Strychnine (Sigma) was dissolved in water and stored at −20 °C. Taurine (Sigma) and β-alanine (Sigma) were also dissolved in water and stored at 4 °C.

Molecular Biology—The human GlyR α1 subunit cDNA was subcloned into the pGEMHE vector. All constructs used in this study contained the functionally silent C41A mutation, which eliminated the sole uncross-linked extracellular sulfhydryl group (19). Site-directed mutagenesis to generate the R19′C, S21′C, and L22′C mutants was performed with the QuickChange mutagenesis kit (Stratagene, La Jolla, CA). Successful incorporation of the mutations was confirmed through automated sequencing of the entire cDNA coding region. The mMessage mMachine kit (Ambion, Austin, TX) was used to generate capped mRNA for oocyte injection. mRNA concentrations were adjusted to 200 pg/nl and aliquots stored at −70 °C.

Oocyte Preparation, Injection, and Labeling—Female *Xenopus laevis* (*Xenopus* Express, France) frogs were anesthetized, and stage VI oocytes were removed from ovaries and washed thoroughly in OR-2 (2.5 mM NaCl, 2 mM KCl, 1 mM $MgCl_2$, 5 mM HEPES, pH 7.4). The oocytes were incubated in collagenase (Sigma) in OR-2 for 2 h at room temperature, rinsed, and stored at 18 °C.

All oocytes were injected with 10 ng of mRNA into the cytosol. To achieve the high levels of expression required for the detection of the fluorescent signal over the background (because of oocyte autofluorescence and nonspecific binding of the dye), the oocytes were incubated for 3–10 days after injection at 18 °C. The incubation solution contained 96 mM NaCl, 2 mM KCl, 1 mM $MgCl_2$, 1.8 mM $CaCl_2$, 5 mM HEPES, 0.6 mM theophylline, 2.5 mM pyruvic acid, 50 μg/ml gentamycin (Cambrex Corp., East Rutherford, NJ), 5% horse serum (Hyclone, Logan, UT), pH 7.4.

To maximize surface expression of receptors prior to labeling, oocytes were incubated at room temperature for 2 h. The oocytes were then transferred into ND96 (96 mM NaCl, 2 mM KCl, 1 mM $MgCl_2$, 1.8 mM $CaCl_2$, 5 mM HEPES, pH 7.4) and stored on ice. For labeling, oocytes were transferred into the labeling solution containing 10 μM MTSR in ND96 for 25 s or 10 μM TMRM in ND96 for 60 min. The oocytes were then washed and stored in ND96 for up to 6 h before recording. All labeling steps were performed on ice.

Voltage Clamp Fluorometry (VCF)—For VCF experiments, an inverted Nikon Eclipse TE300 microscope (Nikon Instru-

TABLE 1

Summary of results for glycine-evoked current and fluorescence recordings

Displayed are the values for half-maximal activation (EC_{50}), Hill coefficient (n_H), number of experiments (n), and maximal current and fluorescence responses (I_{max} and ΔF_{max}, respectively). NA indicates not applicable. All results for fluorescence are shown in boldface.

Construct	EC_{50}	n_H	n	I_{max}	ΔF_{max}	n
	μM			μA	%	
αWT unlabeled	21.5 ± 0.1	2.9 ± 0.1	5	10.0 ± 0.6	NA	9
αWT labeled	19.1 ± 0.1	3.0 ± 0.1	6	8.7 ± 0.6	NA	6
αS21′C unlabeled	21.1 ± 0.1	1.9 ± 0.1	5	6.8 ± 0.3	NA	5
αS21′C labeled	24.3 ± 0.6	1.9 ± 0.1	3	6.2 ± 0.4	NA	3
αS22′C unlabeled	781.0 ± 7.2	1.2 ± 0.1	7	7.3 ± 0.8	NA	7
αS22′C labeled	215.7 ± 0.2	1.9 ± 0.1	6	7.7 ± 0.4	NA	6
αR19′C unlabeled	4450 ± 190	1.7 ± 0.1	7	9.3 ± 1.6	NA	5
αR19′C labeled	994 ± 14	1.7 ± 0.1	7	8.3 ± 0.6	NA	19
αR19′C Δ*F*	**1074 ± 46**	**1.5 ± 0.1**	7	**NA**	**21.4 ± 1.9**	**19**

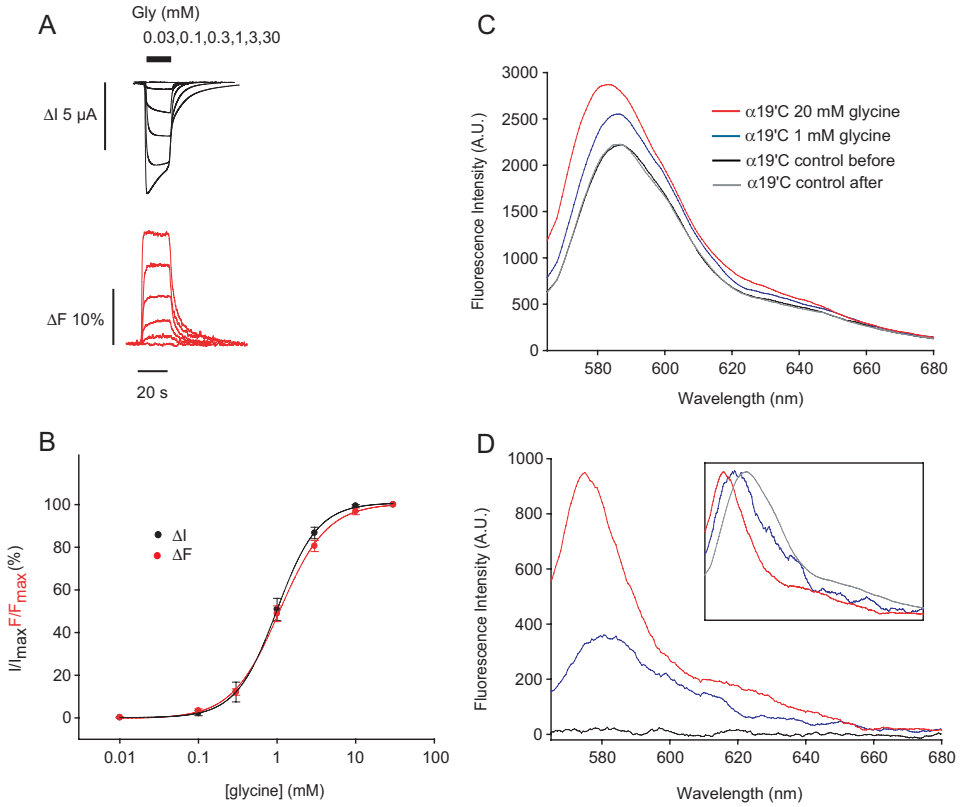

FIGURE 2. **Close coupling of current and fluorescence changes and spectral analysis of MTSR-labeled α1R19′C oocytes.** *A,* glycine-evoked current (*upper panel*) and fluorescence (*lower panel*) recordings from MTSR-labeled α1R19′C oocytes. *B,* glycine dose-response relation for current and fluorescence in MTSR-labeled α1R19′C oocytes. *C,* spectral emission from MTSR-labeled α1R19′C oocytes before, after, and during the application of 1 and 30 mM glycine (average of five cells each). *D,* difference emission spectra from MTSR-labeled α1WT and α1R19′C oocytes recorded during application of glycine. Spectra recorded in the absence of glycine were subtracted from spectra recorded in the presence of glycine (average of five cells). *Red* and *blue traces* were recorded in the presence of 20 and 1 mM glycine concentrations, respectively. The *black trace* shows the difference emission spectrum obtained from a WT-injected oocyte after application of a saturating glycine concentration. *Red* and *blue traces* are shown normalized in the *inset*, along with the spectrum recorded in the absence of glycine (*gray trace*, normalized to the trace obtained with 1 mM glycine).

ments, Kawasaki, Japan) was equipped with a high-Q TRITC filter set (Chroma Technology, Rockingham, VT), a Plan Fluor ×40 objective lens (N.A. 0.6, WD 3.7–2.7 mm) (Nikon Instruments, Kawasaki, Japan), and a PhotoMax 200 photodiode detection system (Dagan Corp., Minneapolis, MN) attached to the side port of the microscope. An excitation filter wheel including a shutter and an emission filter wheel were controlled through a Lambda 10-2 unit (Sutter Instruments, Novato, CA). A Lambda LS 175-watt xenon arc lamp served as a light source and was coupled to the microscope via a liquid light guide (Sutter Instruments, Novato, CA). The design of the custom-made recording chamber is described in Ref. 15. An automated perfusion system operated by a Valvebank 8 module (AutoMate Scientific, San Francisco, CA) was used for perfusion of the recording chamber.

Electrodes for two-electrode voltage clamp recordings were filled with 3 M CsCl and moved by automated ROE-200 micromanipulators coupled to an MPC-200 controller (Sutter Instruments, Novarto, CA). Cells were voltage-clamped at a holding potential of −40 mV in all experiments, and currents were recorded using a Gene Clamp 500B amplifier (Molecular Devices). Current and fluorescence traces were acquired at 200 Hz via a Digidata 1322A interface and Clampex 9.2 software (Molecular Devices). The fluorescence signal was further digitally filtered at 1–2 Hz with an eight-pole Bessel filter for analysis and display. The base line was corrected for bleaching where appropriate. All values for changes in fluorescence indicate an increase in fluorescence, unless stated otherwise. The empirical Hill equation, fitted with a nonlinear least squares algorithm (SigmaPlot 9.0, Systat Software, Point Richmond, CA), was used to obtain half-maximal concentrations (EC_{50} or IC_{50}) and Hill coefficient (n_H) values for ligand-induced activation and inhibition. All results are expressed as means ± S.E. of the mean of five or more independent experiments.

Spectral Analysis—For spectral analysis a MicroSpec 2150i (Acton Research Corp., Acton, MA) coupled to an ORCA-ER CCD camera (Hamamatsu, Hamamatsu City, Japan) replaced the photodiode detection system on the side port of the micro-

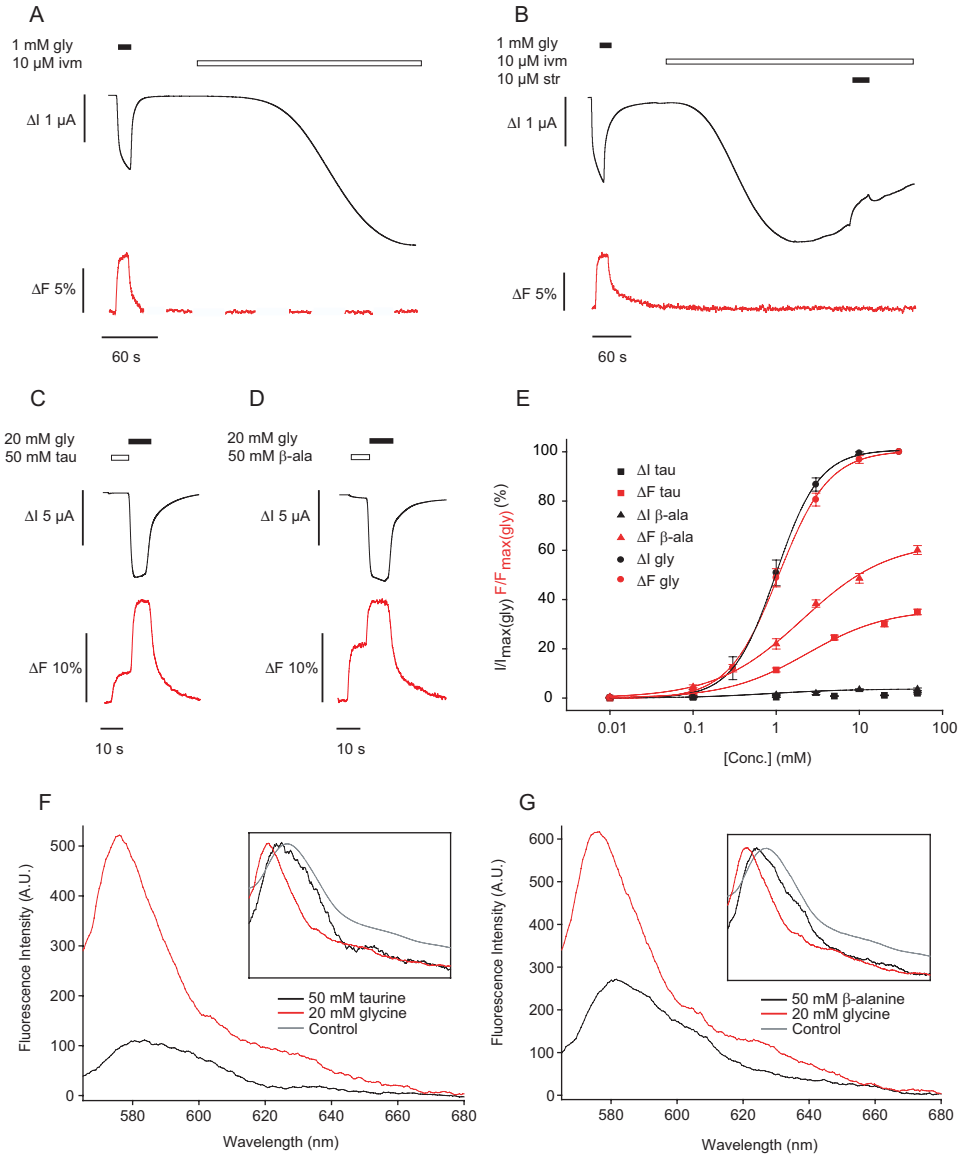

FIGURE 3. **Effects of ivermectin, taurine, and β-alanine on current and fluorescence from MTSR-labeled α1R19′C oocytes.** *A*, current (*upper panel*) and fluorescence (*lower panel*) traces of MTSR-labeled α1R19′C oocyte during glycine (*gly*) and ivermectin (*ivm*) application. The fluorescence recording was interrupted to minimize photobleaching. *B*, current (*upper panel*) and fluorescence (*lower panel*) traces of MTSR-labeled α1R19′C oocyte during glycine, ivermectin, and simultaneous ivermectin and strychnine (*str*) application. *C* and *D*, current (*upper panel*) and fluorescence (*lower panel*) traces of MTSR-labeled α1R19′C oocytes during consecutive saturating glycine (*gly*) and taurine (*tau*) (*A*) or glycine and β-alanine (*β-ala*) (*D*) applications. *Horizontal bars* indicate duration of applications. *E*, current and fluorescence dose-response relations for glycine, taurine, and β-alanine in MTSR-labeled α1R19′C oocytes. *F*, difference emission spectra from MTSR-labeled α1R19′C oocytes recorded during application of saturating [glycine] and [taurine]. *Red* and *black traces* are shown normalized in the *inset*, along with the spectrum recorded in the absence of glycine (*gray trace*, normalized to the trace obtained with 1 mM glycine). *G*, difference emission spectra from MTSR-labeled α1R19′C oocytes recorded during application of saturating [glycine] and [β-alanine]. *Red* and *black traces* are shown normalized in the *inset*, along with the spectrum recorded in the absence of glycine (*gray trace*, normalized to the trace obtained with 1 mM glycine). Difference emission spectra were calculated as described in Fig. 2*D*.

scope. The spectrometer was operated using SpectraPro monochromator software (Acton Research Corp., Acton, MA). For excitation, a HQ535/×50 filter was used in combination with a Q565LP dichroic mirror (Chroma Technology, Rockingham, VT); no emission filter was used. Prior to the experiment, the spectrometer was calibrated using the 434, 546, and 577 nm lines of a mercury lamp spectrum.

To analyze spectra, the image of the region of interest to be monitored was aligned with the slit of the spectrometer. Fluorescence from the region of interest was reflected onto the grating (300 g/mm; 500 nm blaze), and the extracted spectrum was imaged on the ORCA-ER CCD (chip size 1344 × 1024 pixels) using MetaMorph 6.2 (Universal Imaging Corp., Downington, PA). The *x* axis of the resulting "spectral image" represents the wavelength dimension, whereas the *y* axis represents the one-dimensional spatial dimension of the slit. The wavelength coverage for this combination of grating and camera was 170 nm. Adjacent averaging (15 points) was used to smooth recorded spectra (ORIGIN 6.0, Microcal Software Inc., Northampton, MA).

RESULTS

Specific MTSR Labeling of the α1R19′C GlyR—Fig. 1*A* shows examples of glycine-evoked currents recorded from oocytes injected with α1WT RNA (*upper panel*) or mutant α1R19′C RNA (*lower panel*). The averaged glycine dose-response curves are shown in Fig. 1*C*. In this and all subsequent figures displaying dose-response curves, the continuous lines represent fits of the Hill equation to the averaged points. Table 1 shows the mean EC_{50} and n_H values, determined by averaging the parameters determined from curve fits to individual dose responses. Table 1 also shows the mean I_{max} values. As reported previously (20), the α1R19′C mutation results in a dramatically decreased glycine sensitivity. The mean I_{max} was not significantly different in α1R19′C relative to α1WT receptors (9.3 ± 1.6 μA, $n = 5$, *versus* 10.0 ± 0.6 μA, $n = 9$). The effect of MTSR labeling on glycine-evoked currents was also studied. As shown in the example in Fig. 1*B* (*upper panel*), our standard MTSR labeling protocol produced no significant change (+11.7 ± 8.1%, $n = 8$) in the magnitude of currents activated by EC_{10} (5 μM) glycine in α1WT GlyRs (Fig. 1*B*, *upper panel*). However, EC_{10} (1 mM) glycine currents were strongly potentiated in α1R19′C GlyRs following MTSR labeling with a mean current increase of 471 ± 68% ($n = 6$) (*e.g.* Fig. 1*B*, *lower panel*). As shown in Fig. 1*C*, this was caused by a leftward shift in the α1R19′C GlyR glycine EC_{50} value,

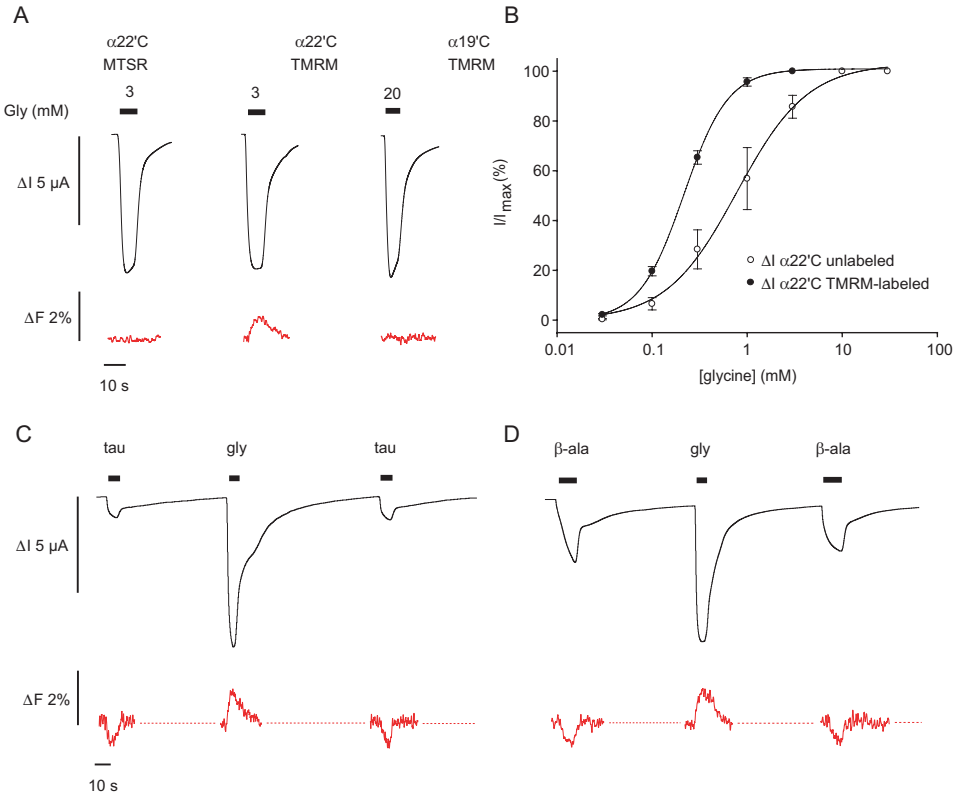

FIGURE 4. **The TMRM-labeled α1L22′C mutant GlyR differentiates between activation by glycine and taurine or β-alanine.** *A,* examples of simultaneously recorded glycine-evoked current (*upper panel*) and fluorescence changes (*lower panel*) from MTSR-labeled α1L22′C GlyRs (*left*), from TMRM-labeled α1L22′C GlyRs (*center*), and from MTSR-labeled α1R19′C GlyRs (*right*). *Horizontal bars* indicate duration of applications. Different fluorophores give different responses when attached to the same residue. *B,* glycine dose-response relations for currents in unlabeled and TMRM-labeled α1L22′C-expressing oocytes. TMRM labeling causes a significant leftward shift in glycine sensitivity. *C* and *D,* simultaneously recorded current (*upper panel*) and fluorescence (*lower panel*) recordings from TMRM-labeled α1L22′C oocytes following the application of 10 mM taurine and 3 mM glycine (*C*) or 10 mM β-alanine and 3 mM glycine (*D*). *Dashed lines* indicate periods of interrupted illumination to prevent photobleaching between applications.

although the n_H remained unchanged (Table 1). As expected, the mean glycine EC_{50} of the α1WT GlyR was not significantly changed by the MTSR labeling procedure (Fig. 1*C* and Table 1). Fig. 1*D* shows a model of three nAChR M2 helices (based on Protein Data Bank code 2BG9), one of which shows the approximate relative locations of the labeled rhodamine[5] and the 9′ leucine residue thought to be part of the channel gate.

Glycine-evoked Changes in Fluorescence Intensity at R19′C—MTSR treatment of oocytes injected with α1R19′C mRNA resulted in an ~3.5-fold increase in resting fluorescence compared with that observed in identically treated uninjected oocytes or oocytes injected with α1WT mRNA (data not shown). VCF experiments showed that glycine application produced changes in fluorescence intensity (Δ*F*) in α1R19′C-injected oocytes that were coincident in time with the activated chloride current (Δ*I*) (Fig. 2*A*), with relative changes in fluorescence (Δ*F*/*F*) regularly reaching 20% at saturating glycine concentrations. In contrast, no significant Δ*F* was ever observed with uninjected or α1WT-injected oocytes. When normalized, the Δ*I* and Δ*F* glycine dose responses were virtually superimposed (Fig. 2*B* and Table 1), strongly suggesting a tight coupling between conformational changes at the 19′ residue and at the channel gate during glycine-induced activation.

Spectral analysis of the fluorescence signal from MTSR-labeled α1R19′C GlyRs revealed that the fluorescence increase was accompanied by an ~10 nm blue shift ($n = 6$) in the MTSR emission peak during full receptor activation (Fig. 2, *C* and *D*). The magnitude of this shift was concentration-dependent, with EC_{50} (1 mM) glycine producing roughly half of the shift produced by a saturating (20 mM) glycine concentration (Fig. 2, *C* and *D*). The blue shift in the MTSR emission peak is characteristic of an increase in hydrophobicity in the fluorophore environment, most likely reflecting a movement of the fluorophore to a more hydrophobic environment in the open state (15). As expected, MTSR-incubated oocytes expressing α1WT GlyRs did not show Δ*F* or spectral shifts (Fig. 2*D*).

Effects of Other Agonists on R19′C Fluorescence Changes—The antihelminthic compound, ivermectin, binds to an as yet unidentified binding site and activates the GlyR in an irreversible manner (21). To confirm the previous conclusion that it activates the GlyR via a different mechanism from glycine (21), we sought to compare the relationship between Δ*I* and Δ*F* produced by ivermectin with that produced by glycine. In MTSR-labeled α1R19′C GlyRs, 10 μM ivermectin evoked slowly developing currents that were roughly double the size of those produced by 1 mM glycine (203 ± 30%, $n = 10$). Despite this large current, no significant increase in the fluorescence intensity was ever observed (*e.g.* Fig. 3*A*). Indeed, the mean fluorescence change in eight oocytes showing robust glycine currents, the Δ*F* response was only 0.5 ± 0.1%. As observed previously (21), the currents evoked by 10 μM ivermectin were only weakly sensitive to strychnine, with 10 μM strychnine reducing current magnitude by 18.9 ± 0.7% ($n = 4$, Fig. 3*B*). No ivermectin-gated currents were observed in uninjected oocytes ($n = 3$). Taken together, these results confirm that ivermectin activates GlyRs by a mechanism different from glycine.

Taurine and β-alanine are low efficacy agonists of α1WT GlyRs, with taurine having a lower efficacy than β-alanine (22). Both compounds are converted into antagonists by a variety of R19′ mutations, including R19′C (20, 23, 24). These actions suggest that taurine and β-alanine bind to the α1R19′C GlyR without activating the receptor and thereby they act as classical competitive antagonists of glycine binding. If this hypothesis is

[5] H. A. Lester and M. I. Dibas, manuscript in preparation.

correct, their binding should not produce significant ΔF. We sought to investigate whether these ligands produced a significant ΔF change upon receptor binding and, if so, whether this was spectrally similar to that produced by glycine. As expected, a 50 mM concentration of taurine did not produce a significant ΔI, although small, nA-sized currents were regularly recorded. Nevertheless, 50 mM taurine produced large changes in ΔF, with a mean value near 35% that evoked by a saturating glycine concentration (Fig. 3*C*). Both ΔI and ΔF stimulated by taurine were completely blocked by 10 μM strychnine (data not shown). Similar results were obtained with β-alanine. A 50 mM concentration of β-alanine evoked only a very small current (~4% that produced by saturating glycine in the same oocyte), but it evoked a large ΔF that was roughly 60% that produced by a saturating glycine concentration (Fig. 3*D*). Again, both ΔI and ΔF stimulated by β-alanine were potently blocked by 10 μM strychnine (data not shown).

The taurine-activated current was too small to be fitted with confidence to the Hill equation (n = 8). However, Hill equation fits to taurine ΔF dose responses (Fig. 3*E*) from the same eight oocytes yielded a mean EC_{50} of 2.4 ± 0.4 mM and n_H of 0.9 ± 0.1. Applications of increasing β-alanine concentrations revealed a close relationship between ΔF and ΔI with no significant differences in their EC_{50} and n_H values (Fig. 3*E*). The ΔF dose response was fitted with a mean EC_{50} of 2.02 ± 0.34 mM and an n_H of 0.8 ± 0.1, whereas the ΔI dose response was fitted with an EC_{50} of 2.61 ± 0.93 mM and an n_H of 1.1 ± 0.4 (n = 6 for each). To facilitate comparison with glycine-mediated responses, Fig. 3*E* also shows the ΔI and ΔF dose response relationships for glycine activation. The fluorescence and current maxima for taurine and β-alanine were both normalized to those produced by glycine in the same oocyte.

Given that the relationship between ΔI and ΔF produced by glycine activation was not preserved during receptor activation by taurine or β-alanine, we hypothesized that these compounds produced different conformational changes at the 19′ residue. We investigated this by measuring the spectral changes produced by both compounds. As shown in Fig. 3*F*, taurine binding produced no detectable spectral shift, whereas the spectral shift produced by β-alanine (~5 nm) was much smaller than that produced by gly-

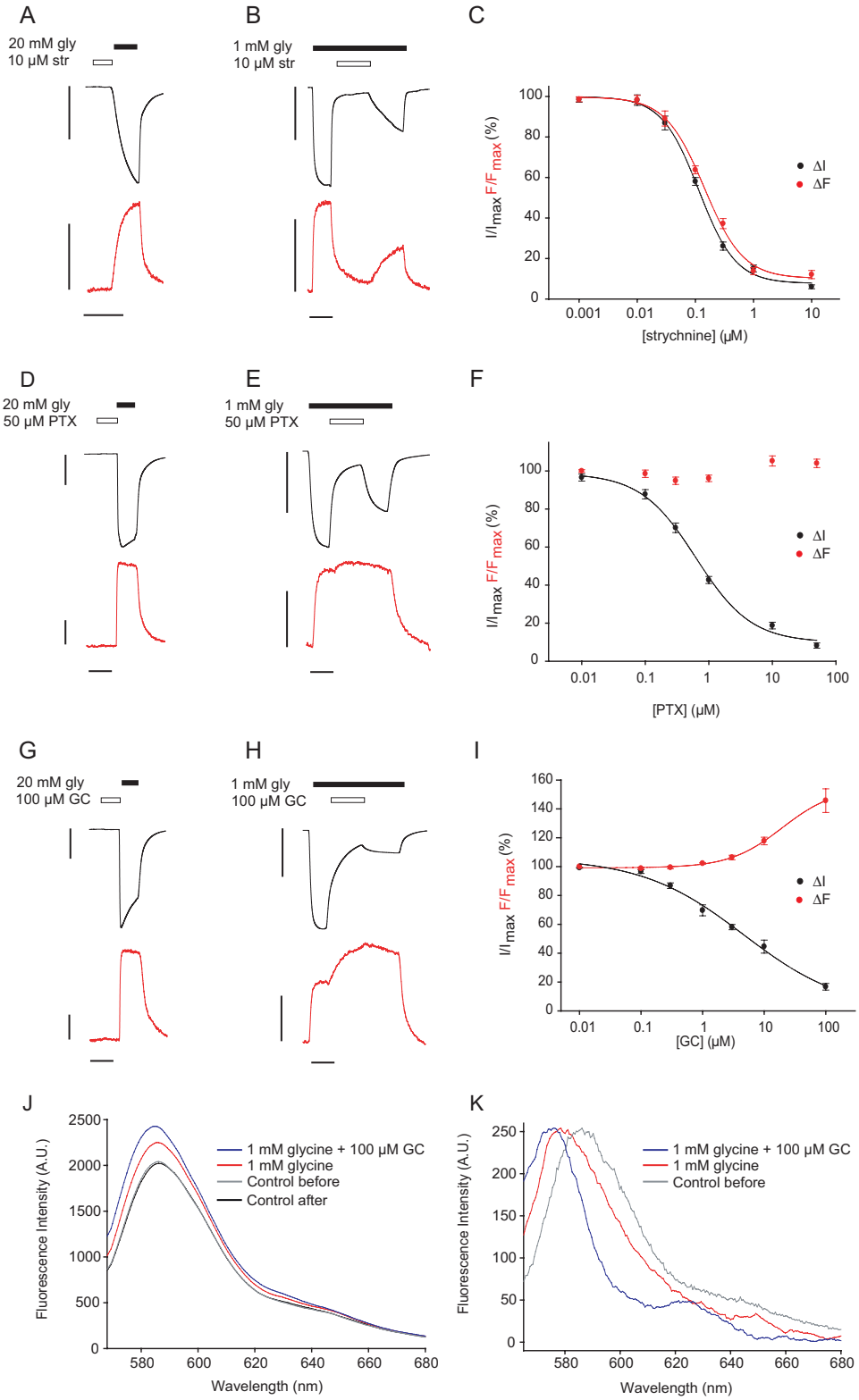

cine (Fig. 3*G*). Together these results strongly suggest that the binding of these weak partial agonists results in different conformational changes from those produced by glycine.

Fluorescence Responses of Other Labeled Residues in the Extracellular M2 Region—As the R19′C mutation impacts severely on receptor function, we assessed whether other cysteine mutants in the extracellular M2 region with less impact on receptor function show a similar pattern of differential responses to different agonists. A previous study (20) showed that cysteine substitutions at the 21′ and 22′ positions disrupt receptor function to a lesser degree than the R19′C mutation. Thus, we focused on these two residues. When injected into oocytes, the α1S21′C GlyR exhibited a WT-like glycine EC_{50}, although the n_H was significantly reduced (Table 1). The α1S21′C-injected oocytes showed no evidence of labeling by either MTSR or TMRM. Incubation with MTSR or TMRM in the presence or absence of 100 μM glycine produced no significant Δ*F* in response to saturating (3 mM) glycine applications ($n = 3$ each; data not shown), and fluorophore labeling produced no change in α1S21′C GlyR electrophysiological properties (Table 1). We conclude that α1S21′C is either not labeled by these fluorophores or that it experiences no change in microenvironment during receptor activation.

The α1L22′C GlyR showed robust expression with electrophysiological properties intermediate between those of α1WT and α1R19′C (Table 1). Importantly, taurine and β-alanine acted as strong partial agonists (see below), as at α1WT receptors. When receptors were labeled with MTSR, no change in Δ*F* could be detected, even at saturating (3 mM) glycine concentrations ($n = 4$) (Fig. 4*A*). However, following labeling by TMRM, α1L22′C-injected oocytes showed a small but significant Δ*F* (1.5 ± 0.3%, $n = 13$) at saturating glycine concentrations (Fig. 4*A*). TMRM labeling also produced a significant increase in the glycine sensitivity of α1L22′C GlyRs (Table 1 and Fig. 4*B*). The small size of these signals precluded quantitation or spectral analysis of the Δ*F* response. In contrast to the effect of glycine, application of saturating (10 mM) concentrations of taurine or β-alanine evoked a significant decrease in Δ*F* (Fig. 4, *C* and *D*). Taurine induced a maximal current of 1.7 ± 0.4 μA and a Δ*F* of −1.1 ± 0.2% ($n = 8$). β-Alanine induced a maximal current of 3.1 ± 0.3 μA and a Δ*F* of −1.1 ± 0.3% ($n = 7$). We then tested whether the sign of the fluorescence change simply depended on the size of the current or was indeed agonist-specific. Application of a low (100 μM) glycine concentration evoked currents of 1.6 ± 0.3 μA ($n = 7$), a value not significantly different from those evoked by 10 mM taurine (1.7 ± 0.4 μA). However, this concentration of glycine produced no significant Δ*F* (0.0 ± 0.1% compared with −1.1 ± 0.2%) ($n = 7$). A similar result was obtained for β-alanine, where currents induced by 300 μM glycine were not significantly different from those evoked by 10 mM β-alanine (3.8 ± 0.6 μA and 3.1 ± 0.3 μA, respectively), but the respective fluorescence changes were significantly different in size and sign (0.3 ± 0.2% compared with −1.1 ± 0.3%; both $n = 7$). Together these results demonstrate that glycine produces a different conformational change at L22′C relative to those produced by taurine and β-alanine.

Effects of GlyR Inhibitors on R19′C Fluorescence Changes—We next sought to compare the effects on the relationship between Δ*I* and Δ*F* of a putative classical competitive antagonist, strychnine, an allosteric inhibitor, picrotoxin, and a putative classical channel blocker, ginkgolide C. The molecular pharmacology of each of these compounds at the GlyR has been reviewed recently (25). When applied alone, strychnine did not evoke significant Δ*I* or Δ*F* changes, even at a concentration of 10 μM (Fig. 5*A*). However, when co-applied with 1 mM glycine, 10 μM strychnine simultaneously decreased Δ*I* and Δ*F* values (Fig. 5*B*). As shown in Fig. 5*C*, the sensitivities of Δ*I* and Δ*F* to strychnine were very similar. Analysis of the strychnine Δ*I* dose-response relationships yielded IC_{50} and n_H values of 114.2 ± 9.4 nM and 1.4 ± 0.1 ($n = 5$), whereas the Δ*F* dose responses were fitted by IC_{50} and n_H values of 142.5 ± 14.4 nM and 1.3 ± 0.2 ($n = 5$). Thus, strychnine itself cannot induce conformational changes that are detectable with a fluorophore attached to α1R19′C, although it can antagonize glycine-induced conformational changes. This response profile is expected for a classical competitive antagonist.

On the basis of a substituted cysteine accessibility analysis, it was recently proposed that picrotoxin can induce a conformational change in the M2–M3 loop that is not produced by glycine (14). We thus hypothesized that picrotoxin may produce a different relationship between Δ*I* and Δ*F* than was produced by glycine. Application of picrotoxin alone did not produce any changes in Δ*I* or Δ*F*, even at a concentration of 50 μM (Fig. 5*D*). Although co-application of 50 μM picrotoxin with 1 mM glycine potently blocked the current, the Δ*F* remained intact (Fig. 5*E*). Dose-response analysis of Δ*I* yielded an IC_{50} of 626.1 ± 11.4 nM and an n_H of 1.0 ± 0.2 (both $n = 6$). However, in the same six oocytes, Δ*F* showed full amplitude over a broad range of picrotoxin concentrations (Fig. 5*F*). This response profile is expected for a classical open state blocker that plugs the pore without

FIGURE 5. **Effects of GlyR inhibitors on current and fluorescence recordings from MTSR-labeled α1R19′C oocytes.** *A,* current (*upper panel*) and fluorescence (*lower panel*) traces of MTSR-labeled α1R19′C oocyte during consecutive, saturating [strychnine] (*str*), and [glycine] (*gly*) applications as indicated by *horizontal bars*. *B,* current (*upper panel*) and fluorescence (*lower panel*) traces of MTSR-labeled α1R19′C oocyte during co-application of EC_{50} [glycine] with saturating [strychnine]. *C,* current and fluorescence dose-response relations for the inhibition by strychnine when co-applied with 1 mM glycine. *D,* current (*upper panel*) and fluorescence (*lower panel*) traces of MTSR-labeled α1R19′C oocyte during consecutive, saturating [picrotoxin] (*PTX*), and [glycine] (*gly*) applications as indicated by *horizontal bars*. *E,* current (*upper panel*) and fluorescence (*lower panel*) traces of MTSR-labeled α1R19′C oocyte during co-application of EC_{50} [glycine] with saturating [picrotoxin]. *F,* current and fluorescence dose-response relations for the inhibition by picrotoxin when co-applied with 1 mM glycine. *G,* current (*upper panel*) and fluorescence (*lower panel*) traces of MTSR-labeled α1R19′C oocyte during consecutive, saturating [ginkgolide C] (*GC*) and [glycine] (*gly*) applications as indicated by *horizontal bars*. *H,* current (*upper panel*) and fluorescence (*lower panel*) traces of MTSR-labeled α1R19′C oocyte during co-application of EC_{50} [glycine] with saturating [ginkgolide C]. *I,* current and fluorescence dose-response relations for the inhibition by ginkgolide C when co-applied with 1 mM glycine. *Horizontal scale bars,* 20 s; *vertical scale bars* (*upper panels*), 2 μA; *vertical scale bars* (*lower panels*), 5% Δ*F*. *J,* spectral emission from MTSR-labeled α1R19′C oocytes before, after, and during the application of 1 mM glycine and 1 mM glycine + 100 μM ginkgolide C (average of five cells each). *K,* difference emission spectra from MTSR-labeled α1R19′C oocytes recorded during application of glycine and glycine + ginkgolide C, respectively. Both the *gray trace* (spectral emission before application of agonist) and the *blue trace* are normalized to the 1 mM glycine emission peak. Difference emission spectra were calculated as described in Fig. 2*D*.

altering the normal open state conformation. Although it provides no evidence to support the previous conclusion for picrotoxin imposing a distinct conformational change in the M2–M3 loop (14), we cannot eliminate the possibility that such a conformational change may occur without a change in hydrophobicity at R19′C.

We next investigated the effects of the GlyR pore blocker ginkgolide C. As with strychnine and picrotoxin, high concentrations (100 μM) of ginkgolide C applied alone did not evoke detectable ΔI or ΔF (Fig. 5*G*). When co-applied with 1 mM glycine, ginkgolide C decreased ΔI but dramatically increased ΔF (Fig. 5*H*). Dose responses averaged from six oocytes revealed an averaged ΔI IC_{50} of 4.6 ± 2.4 μM and an n_H of 0.5 ± 0.1 and an averaged ΔF EC_{50} of 19.6 ± 4.1 μM and an n_H of 1.0 ± 0.1 (Fig. 5*I*). Spectral analysis revealed that the effect of ginkgolide C on the MTSR emission spectrum was similar to that produced by saturating glycine concentrations (compare Fig. 5*K* with Fig. 2*D*, *inset*). An exception is the ginkgolide C-induced hump near 625 nm for which we have no explanation. Overall, the results indicate that pore block by ginkgolide C induces a conformational change in M2–M3 similar to that produced by saturating concentrations of glycine.

Analysis of the Effects of the GlyR Potentiating Agent, Propofol—Propofol is an intravenous anesthetic that potentiates GlyRs by binding to the alcohol and anesthetic binding site located between TM2 and TM3 (26, 27). Its potentiation, particularly of taurine- and β-alanine-gated currents, is facilitated by mutations to R19′ in α1 GlyRs (28). As propofol is hydrophobic and its putative binding site lies in close proximity to the 19′-labeled MTSR, it may directly affect fluorescence by modulating the hydrophobicity of the environment surrounding the fluorophore. However, there was no significant change in the basal fluorescence level when MTSR-labeled α1R19′C GlyRs were incubated with 500 μM propofol for 2 min. Similarly, preincubation with propofol and subsequent MTSR labeling in the presence of propofol (500 μM each) did not change ΔF_{max} or the resting fluorescence intensity (data not shown). Following a 2-min incubation with 500 μM propofol, MTSR-labeled α1R19′C GlyRs retained the ability to produce

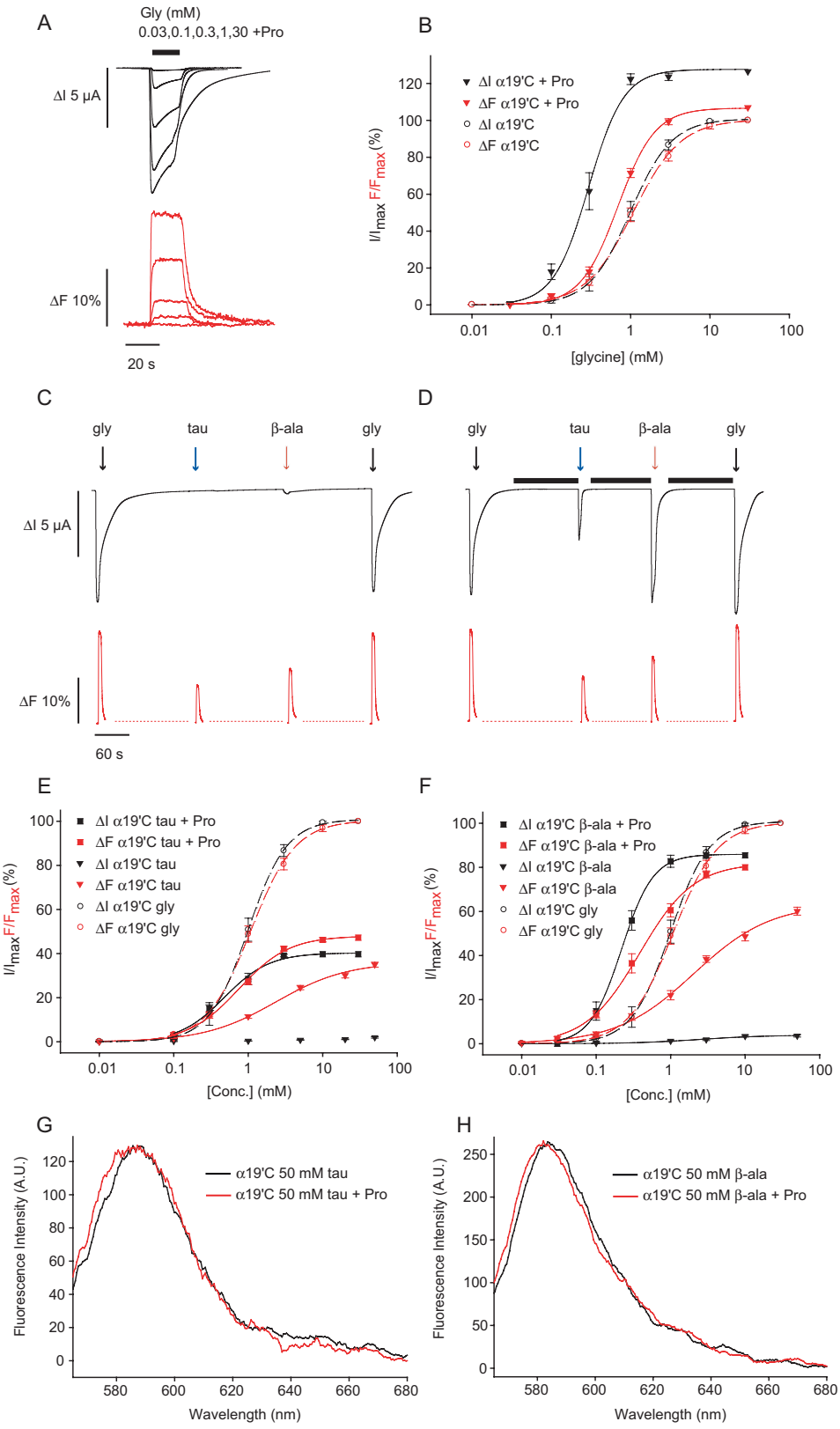

TABLE 2

Summary of results for glycine-, taurine-, and β-alanine-evoked current and fluorescence recordings from MTSR-labeled α1R19′C oocytes

Results are shown for recordings before and after a 2-min preincubation with 500 μM propofol (+PRO). Displayed are values for half-maximal activation (EC_{50}), number of experiments (*n*) and maximal current and fluorescence responses (I_{max} and ΔF_{max}, respectively). All results for fluorescence are shown in boldface.

Agonist	Construct	EC_{50} ΔI	EC_{50} ΔF	n	I_{max}	ΔF_{max}	n
		μM	μM		μA	%	
Glycine	αR19′C	994 ± 14	**1070 ± 46**	7	8.3 ± 0.6	**21.4 ± 1.9**	19
	αR19′C +PRO	419 ± 34	**718 ± 108**	6	10.5 ± 1.2	**22.9 ± 2.7**	8
β-Alanine	αR19′C	2610 ± 927	**2030 ± 344**	6	0.19 ± 0.03	**13.2 ± 1.7**	7
	αR19′C +PRO	219 ± 4	**381 ± 26**	6	7.1 ± 0.4	**17.1 ± 1.1**	14
Taurine	αR19′C	NA	**2350 ± 443**	8	0.04 ± 0.01	**7.6 ± 0.7**	8
	αR19′C +PRO	749 ± 53	**479 ± 49**	5	3.3 ± 0.6	**10.1 ± 0.6**	13

robust current and fluorescence changes in response to increasing glycine concentrations (Fig. 6*A*). Propofol pretreatment significantly increased the ΔI_{max} but not the ΔF_{max} value and significantly reduced the mean glycine EC_{50} values for both Δ*I* and Δ*F* (Fig. 6*B* and Table 2).

The same propofol pretreatment drastically increased the taurine- and β-alanine-mediated Δ*I* responses although their Δ*F* values were less affected (Fig. 6, *C* and *D*). The effects of propofol on averaged Δ*I* and Δ*F* dose responses for taurine and β-alanine are summarized in Fig. 6, *E* and *F*, respectively, with mean parameters of best fit to the dose-response curves summarized in Table 2. As with glycine-mediated responses, the taurine- and β-alanine-mediated Δ*F* EC_{50} values were shifted to significantly lower values. The ΔF_{max} value for taurine was significantly increased by propofol, whereas the corresponding value for β-alanine was not. The ΔI_{max} values for both taurine and β-alanine were also significantly increased by propofol. Considering that propofol converted β-alanine and taurine into highly efficacious agonists, we tested whether their Δ*F* characteristics may have changed to more closely resemble those produced by glycine. Surprisingly, however, propofol had no effect on the spectral maxima of the Δ*F* increases induced by either β-alanine or taurine (Fig. 6, *G* and *H*).

DISCUSSION

Structural Basis for Fluorescence Change—Given the distance of R19′C and L22′C from the glycine-binding site (12) and their position midway along the conformational wave that extends from the binding site to the activation gate upon agonist binding (11), we propose that fluorescence signals arising from rhodamine-labeled R19′C and L22′C are not likely to simply reflect ligand binding. They are more likely to result from a rotation or tilting of the M2 helix during the conformational change that ultimately leads to channel opening. During this global conformational rearrangement, the MTSR fluorophore at the 19′ position may move to a more hydrophobic environment. TMRM attached to L22′C moves into a more hydrophobic environment when activated by glycine, but it moves into a more hydrophilic environment when activated by taurine or β-alanine. However, we cannot rule out the possibility that a quenching group moving toward or away from the fluorophores may contribute to the observed fluorescence changes. Our experiments do not allow us to discriminate among the existing structural models of Cys loop receptor activation, although they do permit us to compare M2 domain conformational changes produced by different ligands.

Agonist-induced Conformational Changes—Perhaps our most dramatic result is that ivermectin activates the pore without producing a significant Δ*F* in the 19′-attached MTSR. Although it has been suggested previously that ivermectin and glycine activate the GlyR pore via structurally different mechanisms (21), the present result provides a much stronger case for this conclusion. The Cys loop receptor ivermectin-binding site is yet to be identified. Being lipophilic, it is possible that ivermectin binds either to a transmembrane or an intracellular site. Regardless of where it binds or how it activates the receptor, it is surprising that ivermectin opens the pore with no detectable change in the conformation at the top of M2. This raises the intriguing possibility that ivermectin produces conformational changes at the internal part of the M2 domain only, perhaps via an interaction with the M1–M2 linker.

Taurine and β-alanine are low efficacy glycinergic agonists that are converted into antagonists by R19′ mutations (20, 23, 24). Although their efficacy at activating GlyR currents was very weak, both ligands evoked large Δ*F* responses that were not accompanied by blue shifts in the spectral emission peak (Fig. 3, *F* and *G*). This response profile differs drastically from that produced by glycine, which was characterized by a close coupling between Δ*I* and Δ*F* and a substantial blue shift in the emission spectral peak. Thus, the conformational change at R19′ produced by these ligands is distinct from that produced by glycine. This is not surprising because it was already evident from their low efficacy that taurine and β-alanine must produce

FIGURE 6. **Propofol effects on glycine-, taurine-, and β-alanine-evoked currents in MTSR-labeled α1R19′C oocytes.** *A,* glycine-evoked current (*upper panel*) and fluorescence (*lower panel*) recordings from MTSR-labeled α1R19′C oocytes after a 2-min preincubation with 500 μM propofol (+*Pro*). *B,* glycine dose-response relation for current and fluorescence in MTSR-labeled α1R19′C oocytes with and without a 2-min preincubation with 500 μM propofol. *C* and *D,* current (*upper panel*) and fluorescence (*lower panel*) recordings from MTSR-labeled α1R19′C oocytes during the application of 30 mM glycine (*black arrows*), 50 mM taurine (*blue arrows*), and 50 mM β-alanine (*red arrows*). *D, black horizontal bars* indicate application of 500 μM propofol. *E,* taurine-evoked dose-response relation for current and fluorescence in MTSR-labeled α1R19′C oocytes with and without a 2-min. preincubation with 500 μM propofol (+*Pro*). *F,* β-alanine-evoked dose-response relation for current and fluorescence in MTSR-labeled α1R19′C oocytes with and without a 2-min preincubation with 500 μM propofol (+*Pro*). *Dashed lines* indicate interrupted illumination to prevent photobleaching between applications. *G* and *H,* difference emission spectra from MTSR-labeled α1R19′C oocytes recorded during application of saturating [taurine] (*G*) and [β-alanine] (*H*) before and after a 2-min preincubation with 500 μM propofol (+*Pro*), respectively. Emission peaks after propofol treatment were normalized to those recorded before propofol treatment. Difference emission spectra were calculated as described in Fig. 2*D*.

different conformational changes to glycine. However, propofol, which drastically increased the efficacy with which taurine- and β-alanine were able to activate Δ*I*, had no effect on the spectral properties of the concomitant Δ*F* (Fig. 6, *G* and *H*). This result is more significant as it shows that taurine and β-alanine produce no Δ*F* spectral change even when they strongly activate the GlyR. This provides a stronger case for taurine and β-alanine activating the GlyR pore via a different conformational change to glycine. However, a weakness in this argument is that the R19′C mutation may have altered structure and function to the extent that the results may not apply to the WT GlyR.

For this reason, we compared the agonist-specific conformational changes experienced by a TMRM attached to the nearby L22′C residue. Again, we found that glycine produced a different Δ*F* response to that elicited by taurine and β-alanine (Fig. 4, *C* and *D*). This shows that the agonist-specific conformational changes do not pertain only to the functionally impaired α1R19′C GlyRs but also to a nearby mutant with functional characteristics that more closely resemble the αWT GlyR.

Together, these results lead us to conclude that different agonists activate the GlyR by producing different conformational changes to the external region of the M2 domain. Thus, the top of M2 seems to display a conformational mobility that is not necessarily coupled to movements of the channel gate. Conversely, opening of the channel gate does not necessarily propagate back to the top of M2.

Antagonists—Strychnine has long been considered a classical competitive antagonist of the GlyR (1). Our finding that strychnine exhibits very similar inhibitory dose response profiles for Δ*I* and Δ*F* is consistent with this notion. By displacing glycine from its site, strychnine prevents glycine from binding and hence from inducing its Δ*F* change.

Picrotoxin is thought to bind in the GlyR pore and to produce inhibition via an allosteric mechanism (25). We recently concluded on the basis of a substituted cystine accessibility study that it changes the M2–M3 loop conformation in a manner that cannot be achieved by glycine (14). If so, then picrotoxin might be expected to alter Δ*F* in a way that cannot be achieved by altering glycine concentration alone. However, we found that Δ*F* produced by picrotoxin plus glycine equals that produced by glycine alone (Fig. 5, *D–F*). This response profile is expected for a classical pore blocker that blocks current flow without altering the open state receptor conformation. However, we cannot rule out the possibility that picrotoxin changes the conformation of the M2–M3 loop in a way that does not involve a Δ*F* change.

Several lines of evidence suggest that ginkgolides bind in the GlyR pore (29–31), but there is no evidence to date that they produce a conformational change upon binding. Ginkgolides thus bind close to the covalently linked fluorophore. The results of Fig. 5, *G–K*, demonstrate that ginkgolide C-induced inhibition is accompanied by both an increase in Δ*F* and a blue shift in the emission spectra maxima. Unexpectedly, ginkgolide C affects Δ*F* at higher concentrations than those affecting Δ*I* (Fig. 5*I*). This is difficult to reconcile with a model that assumes only one ginkgolide molecule binding per receptor. We propose that the Δ*F* changes are mediated by ginkgolide C binding to a discrete, lower affinity site distinct from the well characterized pore blocker site at the 6′ level. In support of this, a molecular docking study identified a putative ginkgolide-binding site near the M2–M3 loop (31). An alternate explanation is that the relatively large size of ginkgolides may force the pore to become stabilized in the activated state. However, the observed discrepancy between the Δ*F* and Δ*I* ginkgolide dose responses is not readily explainable by this model.

Comparison with Previous VCF Studies—Chang and Weiss (17) employed VCF to investigate molecular rearrangements at three positions in and around the recombinant ρ1 γ-aminobutyric acid type A receptor ligand binding pocket. They found that two GABAergic (where GABA is γ-aminobutyric acid) agonists produced a similar pattern of Δ*F* responses at the three labeled positions. Competitive antagonists prevented these Δ*F* changes but also produced distinct Δ*F* responses in the absence of agonist. Perhaps most interestingly, picrotoxin produced a large Δ*F* at one of the labeled positions, providing strong evidence that by binding in the pore it produces global conformational change (17). A more recent study on α1β2 and α1β2γ2 γ-aminobutyric acid type A receptors showed that the Δ*F* magnitude monitored at two binding domain residues exhibited subunit dependence (18). The results from these two studies provide strong evidence for ligand- and subunit-specific conformational changes in the ligand binding domain. However, they provide no information about whether these differential movements translate into different movements at the pore.

Finally, Dahan *et al.* (15) investigated acetylcholine- and epibatidine-mediated Δ*F* and Δ*I* changes at muscle (αβγδ) nAChRs via a rhodamine label attached to the β subunit 19′ position. They concluded that Δ*F* reported a conformational change at the αδ subunit interface. The Δ*F* signal was also modulated by the receptor desensitization status. Together with the present study, these results indicate that the M2 conformation reflects a wide variety of influences, including the identity of the bound agonist, the molecular identity of the labeled subunit, and the desensitization status of the receptor.

Conclusion—VCF recordings reveal that the GlyR agonists, glycine, taurine, and ivermectin, produce different Δ*F* changes at fluorescently labeled 19′ and 22′ residues. The inhibitors, strychnine and picrotoxin, produced Δ*F* and Δ*I* changes as expected for a competitive antagonist and a channel blocker, respectively. On the other hand, the putative channel blocker, ginkgolide C, produced an increase in Δ*F* that may have signaled a direct interaction between MTSR and a low affinity ginkgolide site. Taken together, our results suggest that the GlyR M2 domain responds with distinct conformational changes to the binding of different agonists.

Acknowledgment—We thank Dr. Tim Webb for helpful discussions.

REFERENCES

1. Lynch, J. W. (2004) *Physiol. Rev.* **84,** 1051–1095
2. Miyazawa, A., Fujiyoshi, Y., and Unwin, N. (2003) *Nature* **424,** 949–955
3. Unwin, N. (1995) *Nature* **373,** 37–43
4. Wilson, G. G., and Karlin, A. (1998) *Neuron* **20,** 1269–1281
5. Cymes, G. D., Ni, Y., and Grosman, C. (2005) *Nature* **438,** 975–980
6. Paas, Y., Gibor, G., Grailhe, R., Savatier-Duclert, N., Dufresne, V.,

Sunesen, M., de Carvalho, L. P., Changeux, J. P., and Attali, B. (2005) *Proc. Natl. Acad. Sci. U. S. A.* **102,** 15877–15882
7. Akabas, M. H., Kaufmann, C., Archdeacon, P., and Karlin, A. (1994) *Neuron* **13,** 919–927
8. England, P. M., Zhang, Y., Dougherty, D. A., and Lester, H. A. (1999) *Cell* **96,** 89–98
9. Law, R. J., Forrest, L. R., Ranatunga, K. M., La Rocca, P., Tieleman, D. P., and Sansom, M. S. (2000) *Proteins* **39,** 47–55
10. Cymes, G. D., Grosman, C., and Auerbach, A. (2002) *Biochemistry* **41,** 5548–5555
11. Grosman, C., Zhou, M., and Auerbach, A. (2000) *Nature* **403,** 773–776
12. Unwin, N. (2005) *J. Mol. Biol.* **346,** 967–989
13. Lee, W. Y., and Sine, S. M. (2005) *Nature* **438,** 243–247
14. Hawthorne, R., and Lynch, J. W. (2005) *J. Biol. Chem.* **280,** 35836–35843
15. Dahan, D. S., Dibas, M. I., Petersson, E. J., Auyeung, V. C., Chanda, B., Bezanilla, F., Dougherty, D. A., and Lester, H. A. (2004) *Proc. Natl. Acad. Sci. U. S. A.* **101,** 10195–10200
16. Gandhi, C. S., and Isacoff, E. Y. (2005) *Trends Neurosci.* **28,** 472–479
17. Chang, Y., and Weiss, D. S. (2002) *Nat. Neurosci.* **5,** 1163–1168
18. Muroi, Y., Czajkowski, C., and Jackson, M. B. (2006) *Biochemistry* **45,** 7013–7022
19. Lynch, J. W., Han, N. L., Haddrill, J., Pierce, K. D., and Schofield, P. R. (2001) *J. Neurosci.* **21,** 2589–2599
20. Han, N. L., Clements, J. D., and Lynch, J. W. (2004) *J. Biol. Chem.* **279,** 19559–19565
21. Shan, Q., Haddrill, J. L., and Lynch, J. W. (2001) *J. Biol. Chem.* **276,** 12556–12564
22. Lewis, T. M., Schofield, P. R., and McClellan, A. M. (2003) *J. Physiol. (Lond.)* **549,** 361–374
23. Rajendra, S., Lynch, J. W., Pierce, K. D., French, C. R., Barry, P. H., and Schofield, P. R. (1995) *Neuron* **14,** 169–175
24. Lynch, J. W., Rajendra, S., Pierce, K. D., Handford, C. A., Barry, P. H., and Schofield, P. R. (1997) *EMBO J.* **16,** 110–120
25. Webb, T. I., and Lynch, J. W. (2007) *Curr. Pharm. Des.* **13,** 2350–2367
26. Lobo, I. A., Mascia, M. P., Trudell, J. R., and Harris, R. A. (2004) *J. Biol. Chem.* **279,** 33919–33927
27. Hemmings, H. C., Akabas, M. H., Goldstein, P. A., Trudell, J. R., Orser, B., and Harrison, N. L. (2005) *Trends Pharmacol. Sci.* **26,** 503–510
28. O'Shea, S. M., Becker, L., Weiher, H., Betz, H., and Laube, B. (2004) *J. Neurosci.* **24,** 2322–2327
29. Kondratskaya, E. L., Lishko, P. V., Chatterjee, S. S., and Krishtal, O. A. (2002) *Neurochem. Int.* **40,** 647–653
30. Kondratskaya, E. L., Betz, H., Krishtal, O. A., and Laube, B. (2005) *Neuropharmacology* **49,** 945–951
31. Hawthorne, R., Cromer, B. A., Ng, H. L., Parker, M. W., and Lynch, J. W. (2006) *J. Neurochem.* **98,** 395–407